博士論文（要約）

Developing Effective Code for Building CSL and Approximate CSL Interfaces of Any Two Lattices and Investigating the Phase Behavior in Interfaces of Diamond-structured Materials

（CSL および近似 CSL 粒界作成のための効率的コードの開発とダイヤモンド構造界面における相挙動の研究）

謝　耀枢
(Xie Yaoshu)

Abstract

This thesis is about 1/4 and 3/4 for two topics. The first topic is focused on solving two issues in atomic simulation for interfaces in crystalline materials. The second topic is to extend the research on grain boundary (GB) phases in bcc and fcc metals to diamond-structured materials. Chapter 1 is the introduction explaining the reason to propose this work for these two topics. Chapter 2 is focused on first topic and Chapters 3-7 are for the second topic.

Most materials with important applications in modern times are crystalline materials. Lacking in full understanding of the crystalline interfaces is one of the main barriers to completely control the performances of devices and facilities involving crystalline materials. Atomic simulation is an effective way to investigate structure-property relationship of crystalline interfaces, which has been widely applied to support in studies on both heterogeneous interfaces (HTIs) with importance in many modern devices and GBs existing in many important engineering polycrystalline materials. Two problems exist in current studies on crystalline interfaces. One is lacking in an effective and convenient package capable to build a CSL interface by only input crystallographic indices and cif files. This has hindered many interface engineers from being capable to simulate arbitrary interfaces they observed experimentally. Another is lacking in a package capable to compute the cell of non-identical displacement (CNID) of any CSL. This makes it ineffective to explore GB structures by sampling the complex energy landscape by applying rigid body translation of one crystal respect to the other.

Chapter 2 discusses the algorithm and usage examples of the generated code to solve the two issues mentioned above. The generated code is capable to build an approximate CSL interface of two arbitrary lattices. For showing the usage examples, it has been applied to generate a CSL GB (twinning GB of CuInSe2) from two crystals forming a three-dimensional CSL and to make a CSL (β-Si_3N_4(0001)/Si(111) interface and a CSL (111)Si/(0001)SiC interface from two crystals with only two-dimensional coincidence). These examples presented how this code is in principal capable to be applied to generate an arbitrary CSL or approximate CSL interface satisfying any cases of engineering application to build an interface close to an interface

structure obtained from an experimental observation, or to make a model of any unknown conceptual interface. In terms of convenience, the required parameters to input are simply some lattice indices and cif files of the two crystals forming the interface. Once the CSL interface is generated, the code simultaneously computes its CNID. The importance of applying CNID in CSL GBs and HTIs have also been illustrated in this chapter and the results have shown that applying the CNID can dramatically improve the efficiency in sampling RBT to determine the interface structures especially for asymmetric tilt, twist and mixed GBs, and for HTIs.

Atomic-scaled simulation and experimental observation have suggested that GBs in fcc and bcc metals can exist as multi-phases and perform phase transition. Understanding such behaviour is of importance to fully figure out the property of GBs while extensive previous studies have been only focused on a single phase of GB. Recently, GB complexion has attracted interests which is a phenomenon discovered in some multi-elemental GBs to perform structural transition at elevated temperature. GB complexion has importance as a better understanding of it can help better control the microstructure of these polycrystalline materials. Similar structural transition of GBs has been predicted to also exist in elemental GBs including the GBs of fcc & bcc metals and a recent study has reported a direct observation of coexistence of two copper GB phases under room temperature, providing evidence that elemental GBs can perform phase-like behaviours. Investigating elemental GB phases is helpful to better understand the GB phase (or complexion) phenomenon they are simpler. However, despites that there have been these exciting achievements in finding GB phases in fcc and bcc metals, considering their physical character of mainly having metallic bonds, it is of both scientific and practical importance to extend this research into other elemental materials. Diamond-structured materials are good candidates to do so because they not only possess covalent bond character which can make new insights of this phenomenon which cannot be obtained from the metallic-bonded GBs. It is also of practical importance considering the fact that diamond-structured materials are widely applied in many important modern devices where the GBs play a significant role in affecting their performances.

The results from chapter 3 to chapter 7 will be published in journal.

This research is helpful for more effective interface simulation and has made new insights on understanding the effects of meta-stable GB phases on the properties of materials with covalent bonds.

CONTENTS

1. INTRODUCTION 8

1.1 Importance in Understanding Interfaces in Crystalline Materials 8

1.2 Atomic Simulation for ICMs and Existing Issues 10

1.2.1 Bicrystal Model and CSL Interfaces 10

1.2.2 Issues in Generating Simulation Cells of CSL Interfaces 12

1.2.3 Issues in Determining Interface Structures 14

1.3 Introduction of Grain Boundary Phases 16

1.4 Thesis Structure and Objectives 17

2. DEVELOPING AN EFFECTIVE PYTHON PACKAGE GENERATING ANY CSL INTERFACES. 19

2.1 Operations on lattices 19

2.2 Principles and algorithms finding a CSL or approximate CSL for any two lattices with a determined disorientation. 20

2.3 Computation of CNID 20

2.4 Examples of the Generated Interfaces 20

2.4.1 Generating non-cubic CSL GBs with known geometric information – $\boldsymbol{\Sigma 3}$ CuInSe2 twinning 20

2.4.2 Generating two-dimensional CSL interfaces - $\boldsymbol{\beta}$-Si_3N_4(0001)/Si(111) 20

2.5 Efficiency Promoted by Using CNID 20

2.5.1 Division of GBs in the FZ-GBP 20

2.5.2 Evaluation of the Efficiency Using CNID 20

2.6 Summary 21

3. EXPLORING PHASES (META-STATES) OF DIAMOND-STRUCTURED GBS AT 0K 22

3.1 Importance and Inspiration to Study Diamond-Structured GB Phases 22

3.2 Methods 23

3.2.1 Exploring GB Phases without varying PAD 24

3.2.2 Exploring GB Phases with varying PAD 25

3.2.3 GB Properties and Simulation Model 28

3.2 Results and Discussion **31**
3.2.1 Resulting GB Phases By the Exploring Method Without Varying PAD 31
3.2.2 Resulting GB States By the Exploring Method With Varying PAD 31

3.3 Summary **31**

4. VERIFYING REASONABILITY OF THE EXPLORED META-STABLE GBS BY FIRST-PRINCIPLES SIMULATION 32

4.1 Method **32**

4.2 Results and Discussion **32**

4.3 Summary **32**

5. COMPUTING GB FREE ENERGY AND MONITORING GB STRUCTURAL VARIATION AT ELEVATED TEMPERATURE 33

5.1 Method **33**
5.1.1 GB Free Energy Computation by QHA 33
5.1.2 GB Free Energy Computation by Frenkel-Ladd-Path – Complexity of Temperature Induced Behaviors of the Meta-Stable GBs 34
5.1.3 GB Structure Variation Monitored by Steinhart Order Parameters 38

5.2 Results and Discussion **39**
5.2.1 Simulated Thermal Expansion of Silicon Lattice and the Lattice Free Energy by QHA 39
41
5.2.2 Thermodynamic Stability of GB Phases at Elevated Temperature 42
This part will be published in journal. 42
5.2.3 Temperature-Induced Structural Variation of GB Phase and Pre-melting 42

5.3 Summary **42**

6. PHASE TRANSITION MECHANISM FROM THE META-2 TO GROUND GB THOUGH LOCALIZED STRUCTURAL RECONSTRUCTION 43

6.1 Method **43**
6.1.1 Visualizing the Transformed Meta-2 GB 43
6.1.2 Computing Transition Barrier by Nudged-Elastic-Band (NEB) 43

6.2 Results and Discussion **43**
6.2.1 Phase Transition Mechanism by Localized Structural Reconstruction 43
6.2.2 Effects of Neighboring Structural Units on The Kinetic Barrier of Reconstruction 43
6.2.3 Effects of disorientation on the GB free energy and entropy 43

6.2.4 Dynamic Simulation of the Phase Transition 43

6.3 Summary **43**

7. ELECTRONIC STRUCTURES OF GB PHASES 44

7.1 Method **44**

7.2 Result and Discussion **44**

7.3 Summary **44**

8. CONCLUSION 45

APPENDIX 47

ACKNOWLEDGEMENTS 48

REFERENCE 49

LIST OF PUBLICATIONS 58

1. Introduction

This thesis is mainly focused on two topics. One is to develop a code capable to be applied to treat some issues of inefficiency and inconveniency existing in current research on simulation for interfaces in crystalline materials (ICMs) and to tackle the shortages of previously reported similar codes supporting in this purpose. The other is to investigate the 'phase behavior' in the interfaces (mainly grain boundaries) of the diamond-structured materials. This chapter will introduce 1) the scientific importance in understanding ICMs; 2) issues in conducting atomic simulation for ICMs; and 3) some well-accepted basic concepts of grain boundary (GB) phases and their engineering significances.

1.1 Importance in Understanding Interfaces in Crystalline Materials

Crystalline materials are materials with repeatable arrangements of atoms or molecules, also known as crystals. Crystals well-known in daily life include ice, salt and most metals. They possess repeated arrangements of identical building blocks of respectively water molecules, sodium ions and chloride ions alternately, and metallic atoms. To satisfy the requirement to form ideal perfect crystals, these building blocks in everywhere of the crystals should have uniform separation in every spatial direction and for those made by molecules, the molecules should also possess identical orientation. Such an order is termed as long-ranged order, which is reflected by the ordered shapes of minerals like the cubic ice and salt, the hexagonal emerald and the tetragonal diamond. The term 'long-ranged' order is to distinguish with the 'short-ranged' order existing in another substance known as amorphous. The most well-known amorphous is the glass made of silica (SiO_2). Instead of presenting a long-ranged order, silica only possesses short-ranged or localized order. In glassy silica, oxygen and silicon atoms form localized tetrahedral arrangements but the separation and orientation of these tetrahedrons are almost random or they present orders only in a much smaller scale which cannot be detected by a diffraction experiment. This difference between the extents of structural order in crystals and amorphous contributes to a significant difference in both their mechanical and physical properties. In fact, most materials with important application in modern times are crystals. Both

the structural metals and alloys to bear loads and the functional ceramics and semiconductors serving to provide special functions are mainly existing as crystals. These materials of crystals are termed as crystalline materials.

With the development in materials science and technology, people nowadays are capable to not only directly observe the atomic scale arrangements in a crystal with a high-resolution microscope but also to compute their physical properties using computational simulation to obtain results acceptable accuracy if only their structures are known. However, it still seems to be a long way to eliminate all the barriers to ultimately understand the mechanism of all the materials' properties. One of the most significant internal and intrinsic barriers is the fact that real crystalline materials generally exist as non-perfect crystals. Real crystalline materials have defects in different dimensions including the one-dimensional point defects (vacancies and interstitials) and two-dimensional defects (dislocations and ICMs). The existence of these defects can be a result of the thermodynamic requirement of entropy increase for the crystals to be stable; or inevitably generated during the synthesis or processing of the materials.

While dislocations and point defects do not significantly break the long-ranged order in a crystal, ICMs brings about a remarkably different aspects of effects on the order and regularity in crystalline materials. ICMs includes heterogenous interfaces (HTIs) connecting two crystals of different materials; and homogeneous interfaces (HMIs) connecting two crystals of identical materials with symmetry breaking at the interfaces. Depending on the way of symmetry breaking, HMIs can be further divided into stacking faults (SFs), domain boundaries (DBs) and grain boundaries (GBs), in which GBs are interfaces between two disoriented-crystals and are most popular to exist in real crystalline materials[1]. On one hand, a HTI generates a physical environment distinct from either individual crystal forming this HTI so that HITs themselves can be applied as special materials to provide novel performances which does not exist individually in any single crystals. When Herbert Kroemer was making the Nobel lecture in 2001, he coined the famous phrase that "the interface is the device" which emphasized the

importance of heterogeneous interfaces in any functional device[2]. Examples of these significant interfaces include not only those in the devices which are already commercialized like electrode/electrolyte interface in solid-state lithium batteries[3], and the semiconductor/electrode interface in thin-film transistors[4]. Exploring the interface physics like interface superconductivity[5] is also a key aspect to achieve well-controlled novel quantum materials. On the other hand, most real crystalline materials are polycrystallines containing GBs which often form complex networks packing disoriented grains and this often results in greatly disparate properties from the well-known single crystals[1,6]. Obviously, compared with other crystalline defects, ICMs can exist as much more diverse structures and cause much severer variation from a perfect crystal's structure. Therefore, the disparity in properties of a real material from a perfect crystal caused by existence of ICMs is often more remarkable than that caused by point defects and dislocations. Hence, it is highly desired to understand how interfaces generate unpredicted properties absent in any individual perfect crystal and how they make polycrystallins behave differently from perfect crystals.

1.2 Atomic Simulation for ICMs and Existing Issues

1.2.1 Bicrystal Model and CSL Interfaces

Atomic simulation is an effective way to investigate structure-property relationship of interfaces. Simulation in HTIs have been effectively applied to investigate the impact of these interfaces on performances of many functional devices[7–10]. Compared with HTIs, more extensive studies has been done in GBs including 1) investigating how the GB geometric parameters like disorientation between grains and GB plane orientation affect GB energy [11–14], GB segregation energy [15] and GB mobility[16]; 2) exploring GB phases and simulating phase transition processes [17–19]; 3) understanding the GB faceting behavior [20,21]; and 4) evaluating the stabilization effects of GB segregation [22,23]. Obviously, simulation for GBs is more flexible than that for HTIs.

A main issue in atomic simulation of materials is the gap between the enormous number of atoms in a real material and the limited computing ability of a computer which can only

simulate the behaviours of a limited number of atoms. This issue was often tackled by applying a supercell with periodic boundary conditions (PBDs). One can simulate the behaviour of an ideal material with infinite dimension in certain well-defined directions by applying PBDs in those directions. In this way, atomic simulation of an acceptable number of replicas of lattices can be applied to make reasonable prediction of properties belonging to an infinitely large material once the maximum effective atomic distance in the simulation cell is large enough so that they have nearly no interaction. For interfaces, one often utilizes such supercell of a single interface to study its physical properties, which is a bicrystal model as can be seen in Figure 1.2.1. Generally, one desires to apply PBDs at least in the two dimensions parallel to the interface plane to simulate an infinitely large two-dimensional interface. As for the other dimension perpendicular to the interface, applying a PBD there generates another interface made by the two surfaces away from the interface while applying a non-PBD there generates two free surfaces. Both the conditions are acceptable depending on the purpose and method of simulation.

Applying PBDs parallel to the interface plane brings about requirements that the two crystals must coincide at the interface. Such coincident crystalline interfaces were termed as coincident site lattice (CSL) interfaces. The discovery of CSL interfaces dates back to 1960s when Brandon and Ranganathan reported their work on finding CSL GBs[24,25], which inspired subsequent extensive mathematical work on the crystallographic aspects of interfaces. Famous contributions includes the first textbook on crystalline interfaces from Bollman[26] and the subsequently proposed Bicrystallography by Pond and Vlachavas[27]. The well-developed mathematic tools and promoted computer science provided possibility for appearance of extensive reported atomic simulation of GBs in 1980s, which remarkably promoted understanding of GBs' structure-property relationships[28–33]. Nowadays combing results of atomic observation from high-resolution microscopies and atomic simulation has become a

popular method to ultimately reveal the structure and properties of interfaces. In this way, making simulation cells has become a frequent task in study interfaces.

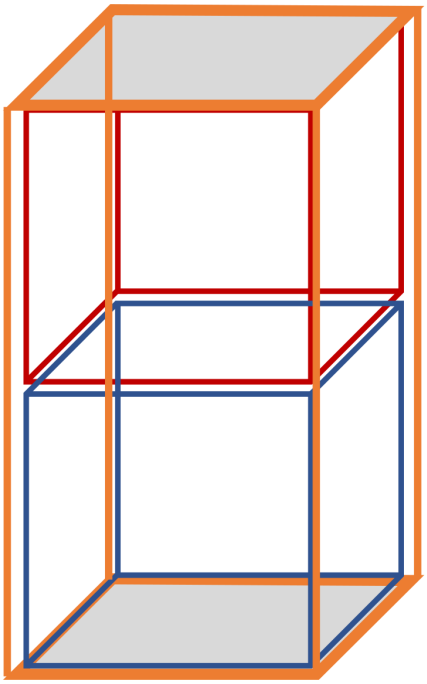

Figure 1.2.1 Bicrystal model of a single interface. Blue and red frames represent two crystals forming the interface. Orange frames are the supercell for simulation. For visualization the orange cell was slightly separated with the two crystals while this separation does not exist in the real simulation. The shaded surfaces of the simulation cell can be set as periodic boundaries or non-periodic boundaries while the other for surfaces were often set as periodic.

1.2.2 Issues in Generating Simulation Cells of CSL Interfaces

Generally, an arbitrary real interface does not have to be a CSL interface. However, CSL interfaces are of great practical importance. Firstly, for many important polycrystalline materials made by a conventional synthesis method, a large proportion of interfaces are CSL interfaces, such as the twinning GBs in many fcc metals. Also, in terms of GB engineering, the performances of polycrystallines can be promoted by manipulate the distribution of CSL GBs[34,35]. Secondly, the CSL HTIs are exact models of epitaxial thin films applied in many

important functional devices[36–39]. Thirdly, a non-CSL interface is possible to be simulated by an approximate CSL interface.

Making a bicrystal simulation cell for a CSL interface requires to define a parallelepiped and specify two sets of lattice directions along the three distinct edges of this parallelepiped. There are two popular cases one desires to conduct simulation of using such cells. One is to simulate discovered interface with information of diffraction pattern or direct observation of atomic structures. The other is to compute a bunch of different GBs in the same materials to reveal the structure-property of GBs distributed in a 'GB space' of two macroscopic parameters including the disorientation $\boldsymbol{D}$ of the two crystals and the GB plane orientation $\boldsymbol{n}$. $\boldsymbol{D}$ can be represented as a linear transformation referring to a rotation operation of one crystal making it identical to the other with 3 degrees of freedom; and $\boldsymbol{n}$ is a unit vector perpendicular to the GB plane with 2 degrees of freedom. The term macroscopic parameters means that they have no information about the atomic structure near the GB and can be known by a diffraction experiment. What is important is that the macroscopic parameters uniquely define a single flat. It is obvious that this single flat GB can further present as different structures. The plane position can shift along the normal of GB plane orientation by a distance d; the two crystals can have relative rigid body translation by a vector $\boldsymbol{t}$. d and $\boldsymbol{t}$ are termed as microscopic parameters with totally 4 degrees of freedom. GBs of identical macroscopic parameter but different in microscopic parameters can be thought as different 'states' or 'phases' of a GB. After specifying all these parameters, the atoms near the GBs will generally be relaxed to a structure which cannot be determined simply from the information of the perfect crystals. Obviously, the proposed possibility of existence of GBs with different microscopic parameter is to say there exist multiplicity of the atomic structures at GBs, which will be one of the main topics of this thesis. Programmes have been reported to make interface supercells while there still exist limitations and usage inconvenience which should and can be promoted by using different computation routines[40–43]. Firstly, most of the generated codes are only available for cubic lattices. For non-cubic lattices, the complexity originates from the fact that deformation of crystals is often needed to form an exact

CSL interface. The package named Pymatgen[43] provide generation of non-cubic CSL GBs while it requires the users to deform the crystals themselves by inputting some rational numbers and the input requirement even varies by different lattice systems which is a non-straightforward and inconvenient usage. Another package named MPInterfaces is capable to find and build the epitaxial interface with lowest mismatch of any two crystal surfaces which provides an effective usage to find the best epitaxial growth conditions. However, it cannot be directly used to make an interface with determined geometry information from a diffraction experiment or build a GB by inputting the macroscopic parameters.

1.2.3 Issues in Determining Interface Structures

As mentioned above, due to the multiplicity of interface structures, a main task is often to tailor the initial bicrystal model to obtain many non-identical and non-relaxed GB structures for subsequent relaxation to explore the GB energy landscape and to obtain the most stable GB structure at 0 K. The operations to tailor the bicrystal often includes applying rigid body translation (RBT) of one crystal respect to the other and others like deleting atoms near the GB which are too close [44]. RBT is an important operation and it is necessary not only in traditional methods for GB structure optimization like the γ-surface method [1], but also in novel methods including Monte-Carlo method [45], generic algorithm [46], and machine learning [14,47,48].

Figure 1.2.3 CSL and DSC lattices. The blue and orange cells are the two overlapping lattices forming the black CSL lattice. The green points belong to the DSC lattice. (This figure will be published in journal)

The effects from applying RBT of one crystal respect to the other on varying the interface structure was firstly discussed by Pond [49] on a tilt CSL GB of aluminium, where the RBT was decomposed to be expressed by two vectors **e** and **p**. **e** is normal to the GB and **p** is confined in the GB plane. RBTs by **e** and **p** adjust the GB structure in different ways. While RBT by **e** simply adjusts the length of vacuum spacing the two crystals, RBT by **p** changes the overlapping two-dimensional pattern that it can introduce remarkable variation of the GB structure. According to Pond [49], if the GB structure possesses a two-dimensional periodicity in

the GB plane, **p** has translational symmetry in cases that the translation by **p** does not relocate the position of GB plane so that it should be reduced into a two-dimensional minimum symmetric unit (MSU). When the GB plane contains only coincident sites (for symmetric tilt GBs), MSU is the Wigner-Seitz (W.-S.) cell of the two-dimensional atomic arrangement of one of the crystals' planes. For more general cases where the GB is not a symmetric tilt GB and its GB plane possesses non-coincident sites, MSU is a displacement shift complete (DSC) lattice [26] of the two overlapping two-dimensional lattices terminated at the GB plane. The general definition of DSC can be understood by Figure 1.2.3 (a), which shows the DSC lattice formed by two overlapping two-dimensional direct lattices. Displacing one of the lattices by a DSC vector presents an identical overlapping pattern with simply a shift of its origin, and therefore displacement included in one DSC unit cell provides all the possible patterns to be non-identical. The DSC in Figure 1.2.3 (a) is a general case where the overlapping lattices do not have to be identical while for symmetric tilt and twist GBs they are identical. Note that for symmetric tilt GBs, their W.-S. cells are equivalent to their DSC lattices. As can be seen, as the DSC is no larger than the Wigner-Seitz (W.-S.), the two-dimensional DSC lattice was also termed as cell of non-identical displacement (CNID) [1]. CNID is important to make effective simulation of CSL interfaces in general cases and it is also essential for understanding other interface-involved concepts and properties such as the GB kinetics [50].

Although CNID belonging to a kind of DSC lattice has a straightforward definition that it is a lattice including both the two disoriented lattices [26], finding a method capable to determine a primitive basis of CNID in general cases can be non-trivial. In some simple cases where the two lattices forming the interface are different only in orientation (e.g. for symmetric tilt and twist GBs), a primitive basis of CNID can be found by directly getting the two shortest non-collinear distance vectors between the two lattices. However, this direct method is not analytic and can be problematic in some complex cases. Up to now, there exists no packages capable to be applied to compute the CNID of an arbitrary CSL interface.

1.3 Introduction of Grain Boundary Phases

Since there exists multiplicity in GB structures, it is plausible to consider whether GBs can behave like a bulk material to exist as multi-phases and perform phase transition. There did exist evidences of GB phases including indirect ones where discontinuous variation of properties were discovered which cannot be explained by phase transitions of the bulk materials[51–53]. Direct evidence for existence of GB phases has also been reported that coexistences of GB phases were directly observed under an atomic-scale-resolution microscopy[54]. Investigation of such phase behaviour is of engineering importance not only because it is related to the synthesis and processing of materials for property promotion but also because it is of great scientific interest to understand the physical importance of the frequently appearing multiplicity of GB structures obtained in atomic simulation.

To avoid confusion, it is necessary to make a definition of GB phases. Here a GB phase is defined as an infinitely large flat single GB which possesses an identical and well-defined set of macroscopic parameters and a uniform distribution of structural identities. Figure 1.3.1 illustrates several cases of coexisting GB phases. This thesis will be focused on the cases of GB phases with the same macroscopic parameter (the same disorientation and GB plane orientation) because such cases have been reported[54–56] and because they present monophase-to-monophase phase transitions which is less complex to investigate. If not specifically specified, all the GB phases mentioned in this article later belong to this case.

Some GB phases can present tiny faceting structures such as one of the well-known silicon GB shown in Figure 1.3.2. Although it possesses faceting structure, it should still be regarded as a single flat GB or a monophase because the faceting steps are not apparent enough to present two well-defined GB plane orientations and neither the steps can individually exist as a single flat GB.

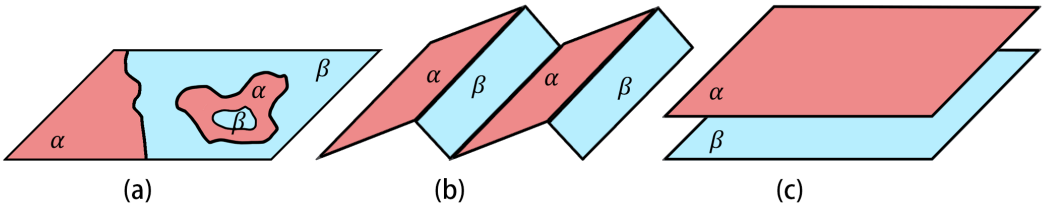

Figure 1.3.1 Cases of coexisting GB phases. (a) GB phases with the same disorientation and GB plane orientation; (b) GB phases with the same disorientation and different GB plane orientation (faceting); (c) GB phases with different disorientation and the same GB plane orientation.

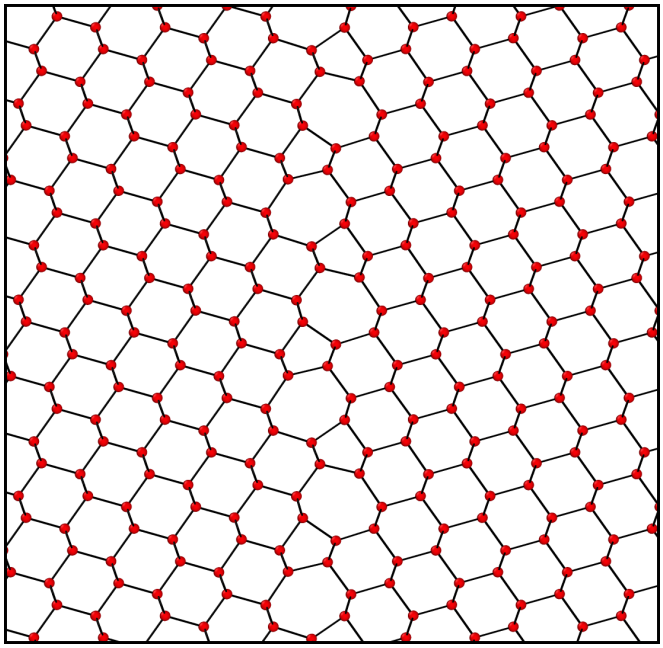

Figure 1.3.2 A silicon GB phase with tiny faceting steps

1.4 Thesis Structure and Objectives

In Chapter 2, I will illustrate the mathematics, algorithm and applications of the developed code. The two main usages including 1) generating a (an approximate) CSL interface of two arbitrary crystals; and 2) computing its CNID will be presented. In Chapter 3, I will explain why this study is focused on the GB phases of diamond-structured GBs. I will present how I apply two methods to explore the phases of the <110>Σ9$(2\bar{2}\bar{1})$ GB and compare explored phases with GB phases in the fcc and bcc metals explored by similar methods and discuss the reason causing the difference between them. Since I explored an enormous number of meta-stable GB phases,

in Chapter 4, I will show the results of DFT simulation of some selected GB phases including one with the lowest grain boundary energy denominated as the Ground GB and three meta-stable GBs as Meta-1, Meta-2 and Meta-3 GBs. They commonly exist in silicon, germanium and carbon. The DFT results will show that they are reasonable structures and thus possible to exist in the real materials. In Chapter 5, I will firstly discuss the thermodynamic stability of the four selected GB phases of silicon through their GB free energy computed by quasi-harmonic-approximation. I will also illustrate the temperature-induced structural variation starting from these phases at 0K through computing the free energy of the system by Frenkel-Ladd-Path and through monitoring their structural similarity by excess Steinhart order parameters. Through the results, I will discuss how to understand the effects of meta-stable phases on the thermodynamic property of a real GB in the diamond-structured materials through the difference in the temperature-induced behavior of selected silicon GBs. These results will also show that the Meta-2 GB is capable to transform to a structure similar with the Ground GB. In Chapter 6, I will show the mechanism of this transition. In Chapter 7, I will show how the phase transition affects the electronic structures to make insights on the effects of GB phases on their polycrystalline physical properties.

2. Developing an effective python package generating any CSL interfaces.

In this Chapter, the algorithms and usages will be explained of the generated python code supporting in generating CSL or approximate CSL interfaces and computing CNID

2.1 Operations on lattices

For better understanding, before introducing the algorithms, some linear operations which will frequently present latter is explained here. There are mainly two operations involved including *Linear Transformation (LT)* and *Supercell Extraction (SE)*.

In this thesis, we will describe all the lattices by a matrix with three column vectors $\boldsymbol{L} = [\boldsymbol{a}, \boldsymbol{b}, \boldsymbol{c}]$. Without special notification, all the vectors are represented in a global cartesian coordination. For an arbitrary lattice defined by three lattice vectors $\boldsymbol{L} = [\boldsymbol{a}, \boldsymbol{b}, \boldsymbol{c}]$, a *LT* is to left-multiply it by a 3x3 matrix $\boldsymbol{T}$ which ends up with a new lattice $\boldsymbol{L_T} = [\boldsymbol{Ta}, \boldsymbol{Tb}, \boldsymbol{Tc}]$. As can be seen, the *LT* operation is applied to all the vectors independently giving the lattice vectors forming the new lattice. On the other hand, a *(SE)* operation is to right-multiply the lattice by a 3x3 matrix $\boldsymbol{U}$. The resulting lattice $\boldsymbol{L_E}$ is:

$$\boldsymbol{L_E} = \boldsymbol{LU} = [\boldsymbol{a}, \boldsymbol{b}, \boldsymbol{c}] \begin{bmatrix} h_1 & h_2 & h_3 \\ l_1 & k_2 & k_3 \\ k_1 & l_2 & l_3 \end{bmatrix} = [\boldsymbol{a_E}, \boldsymbol{b_E}, \boldsymbol{c_E}] \qquad 2\text{-}1$$

where

$$\begin{aligned} \boldsymbol{a_E} &= h_1\boldsymbol{a} + l_1\boldsymbol{b} + k_1\boldsymbol{c} \\ \boldsymbol{b_E} &= h_2\boldsymbol{a} + l_2\boldsymbol{b} + k_2\boldsymbol{c} \\ \boldsymbol{c_E} &= h_3\boldsymbol{a} + l_3\boldsymbol{b} + k_3\boldsymbol{c} \end{aligned} \qquad 2\text{-}2$$

Therefore, the resulting vectors by *(SE)* are three sets of linear combinations of the old lattice vectors where the coefficients are column vectors of the *SE* operation matrix.

2.2 Principles and algorithms finding a CSL or approximate CSL for any two lattices with a determined disorientation.

2.3 Computation of CNID

This part will be published in journal.

2.4 Examples of the Generated Interfaces

This part will be published in journal.

2.4.1 Generating non-cubic CSL GBs with known geometric information – Σ3 CuInSe2 twinning

This part will be published in journal.

2.4.2 Generating two-dimensional CSL interfaces - β-Si_3N_4(0001)/Si(111)

This part will be published in journal.

2.5 Efficiency Promoted by Using CNID

This part will be published in journal.

2.5.1 Division of GBs in the FZ-GBP

This part will be published in journal.

2.5.2 Evaluation of the Efficiency Using CNID

This part will be published in journal.

2.6 Summary

In this Chapter, the generated code building an approximate CSL interface of two arbitrary lattices have been applied to generate CSL GBs from a 3D-CSL (twinning GB of CuInSe2) and 2D-CSL (β-Si_3N_4(0001)/Si(111) interface and (111)Si/(0001)SiC interface). In principle this code can be applied to generate an approximate CSL interface satisfying any cases of engineering application to build an interface close to an interface structure obtained from an experimental observation; or for any unknown interface by simply input lattice indices and cif files with comprehensive usage.

Once the CSL interface is generated, the code simultaneously computes its CNID. The importance of applying CNID in CSL GBs and HTIs have been illustrated and the results have shown that applying the CNID can dramatically improve the efficiency in sampling RBT to determine the interface structures especially for asymmetric tilt, twist and mixed GBs, as well as for HTIs.

3. Exploring Phases (meta-states) of Diamond-Structured GBs at 0K

This chapter discuss the methods and results for exploring GB phases in diamond-structured materials including silicon, germanium and diamond-carbon. I will also compare my results with previously reported GB phases in fcc and bcc GBs.

3.1 Importance and Inspiration to Study Diamond-Structured GB Phases

An interesting discovery of GB phases is that according to the results from atomic simulation, multiple GB phases seem to commonly exist in GBs of fcc metals[17,57]. Inspired from fcc metals, GB phases were subsequently discovered in bcc metals by simulation as well. Successful discovery of GB phases by atomic simulation were later supported by an direct observation of coexisting GB phases of copper under room temperature[54]. Studies on GB phases of elemental materials avoid complexity from involving effects of composition and can individually investigate the GB behaviours under a unique species of chemical bonds. Despites the exciting achievements in fcc and bcc metals mainly with metallic bonds, relevant work has not been reported in other elemental materials, in which one of the most important species includes the diamond-structured materials with covalent bonds whose GBs also have notable effects on performances of many functional devices like solar cells and transistors[58–60].

Although compared with fcc and bcc GBs, few reported studies have applied the term 'GB phases' on diamond-structured GBs, some properties related to phase behaviors have been discussed. Firstly, computational work has suggested that silicon GBs have enormous meta-stable states[61] and their most stable structures can be obtained by reconstruction from those of certain meta-stable GBs[62]. Secondly, molecular dynamics simulations have shown that several different twist GBs of silicon whose structures were optimized at 0K by a molecular dynamic (MD) simulation[63] have different temperature-induced transitions, where some GBs disorder as the temperature raises while some can possess a highly ordered structure even at a high temperature close to pre-melting of the GB[64]. Considering these two aspects, there still exist interesting properties which have not been revealed yet. While previous studies by applying

empirical atomic potentials have explored many GB states or phases of silicon at 0K[61,65], only the reasonability of the most stable GBs were verified by first-principles computation. As for the explored meta-stable GBs as the by-product, they were often ignored and were thought to be unstable in a real material. However, there has been reported experiments verifying existence of meta-stable GBs. For example, one has observed a meta-stable GB containing a 5-fold coordinated atom in a $\Sigma 3$ twinning GB of silicon[66]. Also, while the reconstruction from meta-stable GBs to the most stable GBs were predicted by comparing their atomic structures, rare previous studies have deeply investigated this reconstruction process. The integrated behavior of the localized reconstruction of each unit structures belonging to a two-dimensional GB still remains unknown. Therefore, it is of importance to investigate the reasonability of these meta-stable GBs and the transition process from them to the most stable GBs for the diamond-structured GBs.

3.2 Methods

The methods exploring GB phases are similar to extensive previous studies applied for GB structure optimization, where many different initial configurations obtained by manipulating the CSL GBs by certain operations. These operations are conducted to sample as much as wide area of the phase filed of a GB where many local minimums exist in order to find the local minimum corresponding to the most stable GB structure. For bcc and fcc metals, these operations often include RBT of which the importance has been discussed in **Introduction** and deletion of atoms near the GB. The deletion of atoms is often controlled by varying the cut-off distance that atoms near the GB from different crystals which are closer than this distance will be deleted. However, recent reports have shown that some important GB states or GB phases can only be explored with a special method to control this atom deletion operation, which is to delete the atom so that the atomic density with respecting to a complete GB plane (denoted as planal-atomic-density (PAD)) can be varied. In a simulation cell of a symmetric tilt CSL GB, the number of atoms in the cell n must divide by the number of atoms in a complete GB N. If the atom deletion is controlled by the cut-off distance, for a symmetric tilt CSL GB, the deletion

operation always delete complete planes of atoms so that the PAD *n'%N/N* is always 0. Therefore, previous studies exploring fcc and bcc GB phases[17,54,55] applied other methods to manipulate PAD and they found that when expressing GB energy as a function of PAD, there exist different cusps in the function figure where these cusps are corresponding to different GB phases which can perform phase transition. In this research, I applied both methods with and without varying PAD to explore GB phases in diamond-structured materials. All the initial structures generated to explore GB phases were relaxed through LAMMPS[67] with atomic interactions modeled by with a modified Tersoff potential by Pun and Mishin for silicon[70] , and Tersoff potential for germanium[71] and a long-range bond-order potential for diamond-carbon[72].

3.2.1 Exploring GB Phases without varying PAD

Different from fcc and bcc metals, diamond structured materials have covalent bonds so that the atoms in a reasonable defected structure are expected to have four-fold coordination. Therefore, it is plausible to assume that many reasonable GB phases can be explored without deleting atoms. Note that deleting atoms controlled by cut-off distance can change the coordinate number of atoms to be not four-fold without changing PAD, because number of atoms in a complete GB plane can be not a multiple of four. Therefore, deleting atoms without PAD can result in some coordinate-defected structure. Such coordinate-defected structure has been previously reported in silicon GBs while most previous studies conducting GB simulations often regarded them as non-reasonable structures. Their reasonability remains to be investigated and there for the explored defected GBs by this method provided possibility to do so. Another advantage not to vary PAD is that because all the atoms in the same GB plane of a symmetric tilt GB are in equivalent positions, this method guarantees that every the relax structure have a well-defined structural unit. This is crucial to define GB phases because different GB phases can be identified by their own structural units that only pure phases were generated without mixed phases. This method was applied to explore GB states of silicon, germanium and carbon by relaxing a series of non-identical initial configurations obtained by tailoring a bicrystal model of the <110>$\Sigma 9(2\bar{2}\bar{1})$ GB in molecular dynamics (MD) simulation at 0 K. This Σ9 GB

was selected because it not only is a popular GB in polycrystallines[73] of silicon but also has its most stable structures well studied by simulation[62,65]. Before conducting atom deletion, RBT in one periodicity of CNID is sampled in a mesh size of about 0.03 lattice parameter. The exploring process is nearly identical for all the three different elements with different lattice parameters, each resulting in about 33700 initial configurations to be relaxed.

3.2.2 Exploring GB Phases with varying PAD

This research also explored different GB states with varying PAD for silicon GBs. Previous studies for fcc GBs do this through merging atoms one-by-one[17] near the GB or using more advanced methods like generic algorithms[54,55,74]. Here, I applied the merging-atom method. The process of this method is shown in Figure 3.2.2 (a). For each operation, the two closest atoms near the GB are merged at the equivalent middle-point of them. This operation runs until the distances between all the atoms is larger than 0.99 times the closest atomic distance in a perfect diamond structure. Like that in 3.1.1, RBT in the CNID was also sampled. Specially, considering the fact that in diamond-structured crystal, there exist two motifs per lattice point, denoted as A and B. Therefore, three different terminating conditions of A plane - A plane, A plane – B plane, and B plane – B plane were applied as shown in Figure 3.2.2 (b)

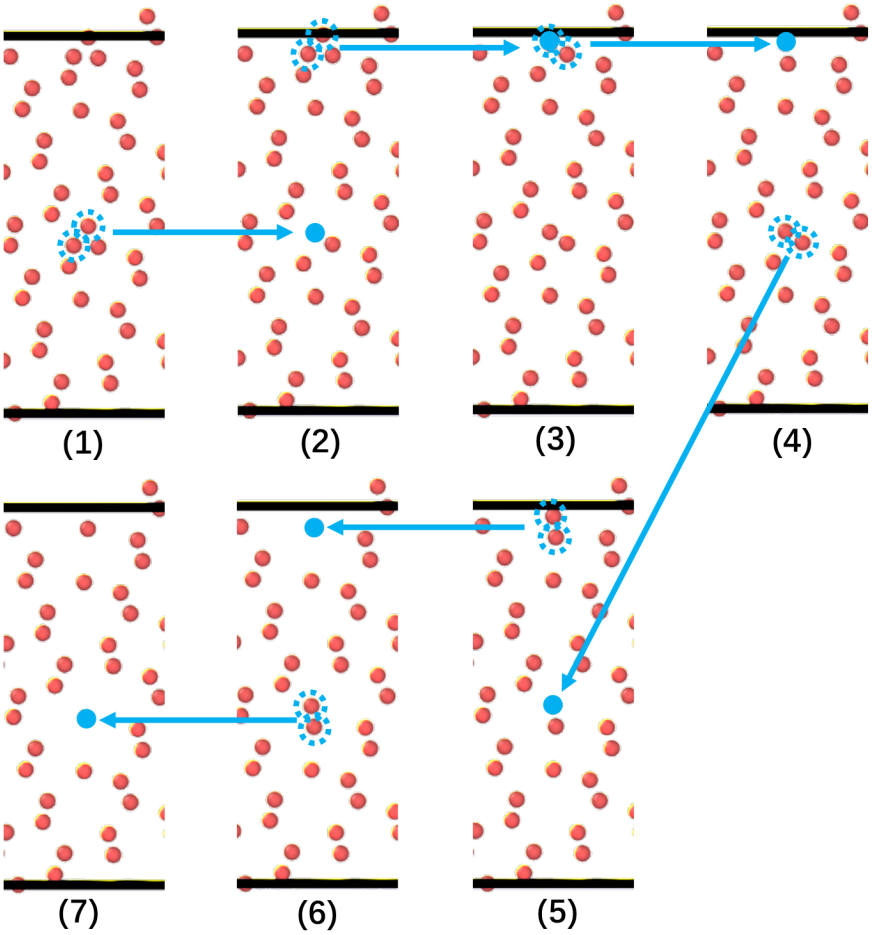

Figure 3.2.2 (a) The process emerging atoms one-by-one to vary PAD.

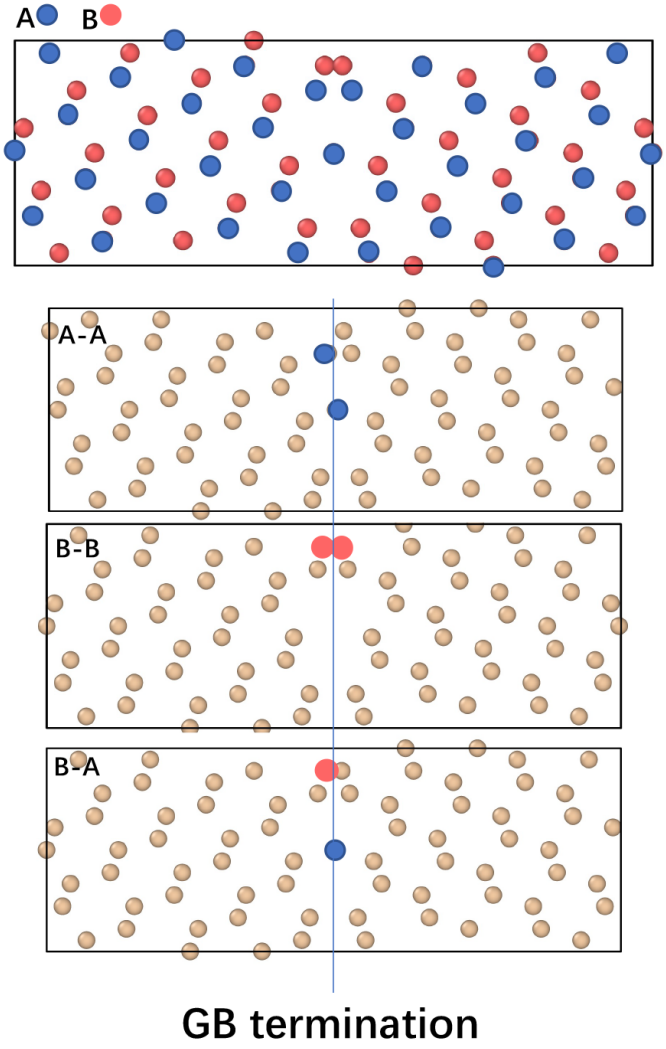

Figure 3.2.2 (b) Three different terminating conditions.

3.2.3 GB Properties and Simulation Model

If a GB is assumed to be a multi-phase system, it is of high importance to investigate the property distribution at 0K of these different phases. As will be shown later, this is even important for diamond-structured GBs because compared with fcc and bcc metals they possess far more GB states or phases. On one hand, due to effects of entropy, the free energy of unstable state at 0K can appear in elevated temperature. On the other hand, due to existence of kinetic barriers, some meta-stable states can be kinetically trapped at certain temperature. Therefore, the GB property distribution at 0K can be regarded as a pool of accessible states or phases of this GB system in a real environment. Similar to the method applied in previous studies on fcc and bcc GB phases[17,55] and according to the work of Frolov & Mishin[75], for each relaxed GB, I computed several GB excess properties including the excess GB energy [E], the excess order parameters [Q_3] [Q_6] [Q_7], the GB stress [τ_{11}], [τ_{22}], and the excess volume [V]. The definition of excess property [Z] is

$$[Z] = (Z_g - N_g/N_b Z_b)/A \tag{3-1}$$

where Z_g is the sum of property Z in a region with a size large enough to contain the complete GB structure and its affecting neighboring atoms which are in different environment from in a bulk; N_g is the number of atoms in this GB region; Z_b, N_b are the sum of the property Z in a perfect bulk and the number of atoms in it; . Therefore, the excess property [Z] of a GB is the 'excess value' of property Z caused by existence of that GB. For all the selected excess properties, [Q_3] [Q_6] [Q_7] were computed to quantify the structural similarity of computed GBs (see Appendix 2 for more details about order parameters) and other intensive parameters [E] [τ_{11}] [τ_{22}] [V] are computed because they are intrinsic properties of each GB corresponding to the adsorption equation of a symmetric tilt GB in an elemental material under stress[75]:

$$d(\gamma A) = -A[S]dT - A[V]d\sigma_{33} - A\sum_{i=1,2} B_i\, d\sigma_{3i} + A\sum_{i=1,2} \tau_{ij} de_{ij} \tag{3-2}$$

B_i, σ_{3i}, e_{ij} are parameters to describe the stress and strain condition of a bicrystal model of a symmetric tilt GB, for which the 1-axis is the tilt axis; 2-axis is along the direction constrained in the GB plane and perpendicular to the 1-axis; 3-axis is perpendicular to the GB plane, as

shown in Figure 3.2.3 (a). B_i is the relative shear distance of the two 3-surfaces; σ_{3i} is the shear stress applied in the two 3-surfaces; e_{ij} is the strain constrained in the GB plane. τ_{ij} is a complex parameter which according to Frolov & Mishin[75] is 'the excess of lateral components of the stress tensor relative to their values inside the grains'. When there is no stress applied to the 3-surfaces ($\sigma_{3i} = 0$), which is true for our simulation exploring GB phases at 0K, 3-2 becomes

$$d(\gamma) = -[S]dT - [V]d\sigma_{33} + \sum_{i=1,2}[\tau_{ij}]de_{ij} \qquad 3\text{-}3$$

where

$$[\tau_{ij}] = \left(\overline{\sigma_{ij}}_g V_g - \frac{N_g}{N_b}\sigma_{ij}{}_b V_b\right)/A \qquad 3\text{-}3$$

$\overline{\sigma_{ij}}_g$ is the 'averaged stress' of the GB region with volume V_g, $\sigma_{ij}{}_b$ is the stress of a homogeneous bulk region in the simulation cell with volume V_b.

The simulation cell is shown in 3.1.3 (b). The dimension in the direction perpendicular to the GB plane is consistent to be multiples of minimum orthogonal CSL lattice until reaching a length over 100 angstroms for each crystal. For exploring method mentioned in 3.1.1 the dimension in the GB plane is a multiple of 6×6 the minimum orthogonal CSL lattice while for the method in 3.1.2, a range of different dimensions including [Ny, Nz] = [2, 1], [6, 1], [7, 2], [9, 2], [11, 2], [13, 2] are applied to sampling as many as values of PAD.

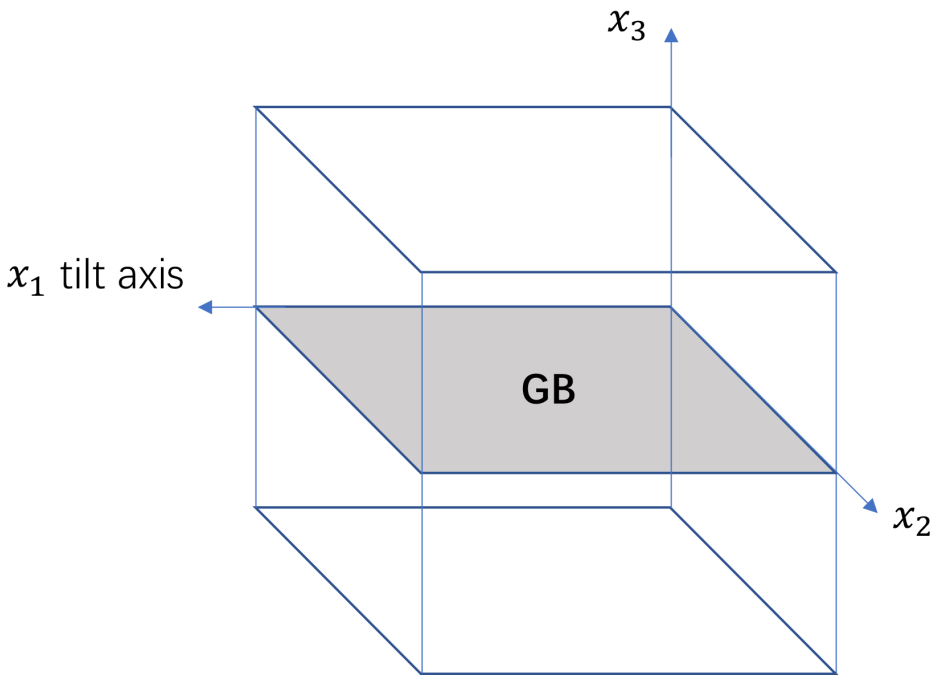

Figure 3.2 .3 (a) Assigning stress & strain descriptions in a bicrystal mode of GB.

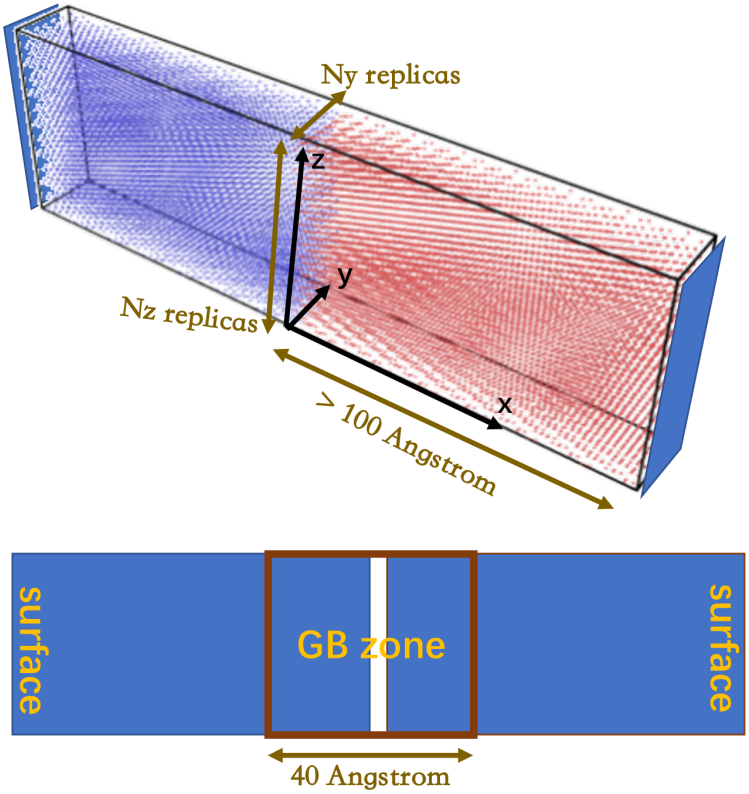

Figure 3.1.3 (b) The simulation cell.

3.2 Results and Discussion

3.2.1 Resulting GB Phases By the Exploring Method Without Varying PAD

This part will be published in journal.

3.2.2 Resulting GB States By the Exploring Method With Varying PAD

3.3 Summary

This part will be published in journal.

4. Verifying Reasonability of the Explored Meta-stable GBs by First-Principles Simulation

Considering that the empirical atomic potential applied for MD simulation is often based on the perfect crystal model and can be questionable when being applied to the GB structure which is defected, I conducted first-principles simulation using density-functional-theory (DFT) method to verified for some explored GBs by MD simulation. This chapter will discuss the method and result of this simulation, which well verified the reasonability of some explored meta-stable GBs.

4.1 Method

This part will be published in journal.

4.2 Results and Discussion

This part will be published in journal.

4.3 Summary

This part will be published in journal.

5. Computing GB Free Energy and Monitoring GB Structural Variation at Elevated Temperature

As I have verified the reasonability of the meta-stable GBs to exist in diamond-structured materials, it is then of interest to reveal their phase behaviors. In previous studies, the meta-stable GBs have not been considered as important structures because they were often thought unstable and will transform to the 'ground' state in a real environment. However, this might be problematic. Firstly, due to the entropy effects, the difference between the free energy of meta-stable GBs and the ground-stable GB is possible to be compensated at elevated temperature. Secondly, the process of a meta-stale GB accidently generated during the synthesis or processing of materials transforming to the ground-stable GB is possible to be kinetically trapped which is especially highly like to be the case in diamond-structured materials. As I have discussed in 3.2.1, the localized instability in diamond-structured materials is difficult to be relaxed if the relaxation involves diffusion. This chapter discuss the GB free energy of the four selected GBs shown in 4.1 at elevated temperature by quasi-harmonic approximation (QHA) and Frenkel-Ladd-path method; and the variation of their excess order parameters. The free energy computed by QHA is capable to show the relative stability of different GB phases at elevated temperature. The free energy computed by Frenkel-Ladd-path method and the variation of excess order parameters are used to illustrate the structural variation of them. The method applied for GB free energy computation was proposed by Rodrigo[82].

5.1 Method

All the MD simulations involved in this part applied a Langevin benchmark for simulating atomic vibrations at elevated temperature. The time step is 1 fs. Without specification, all the simulations were done in a fixed volume condition.

5.1.1 GB Free Energy Computation by QHA

For a system described by a Hamiltonian as

$$H_0 = \sum_{i=1}^{N} \frac{\boldsymbol{p}_i^2}{2m} + U(\boldsymbol{r}_1, \boldsymbol{r}_2, \dots, \boldsymbol{r}_N) \qquad 5\text{-}1$$

Its free energy by quasi-harmonic-approximation can be analytically determined as

$$F(N,V,T) \approx U(N,V,T) + \sum_{n=1}^{3(N-1)} \ln\left(\frac{\hbar\omega_n(T)}{k_B T}\right) \quad 5\text{-}2$$

$\omega_n(T)$ are the phonon frequencies which are functions of temperature. For harmonic approximation (HA), $\omega_n(T)$ is a constant determined by $\omega_n(0)$. For QHA, the temperature dependency of ω_n is reflected by manipulating lattice parameter to accompany thermal expansion, and it is computed through a static system using the dynamic matrix with components computed using LAMMPS:

$$D_{i,j}^{\alpha,\beta}(T) = \frac{1}{m}\left(\frac{\partial^2 U}{\partial r_{i,\alpha}\partial r_{i,\beta}}\right)_{r=r_0(T)} \quad 5\text{-}3$$

$\omega_n(T)$ are eigenvalues of $\boldsymbol{D}(T)$.

The GB free energy was computed as excess free energy

$$F_{GB} = \frac{F_g - N_g F_L}{A} \quad 5\text{-}4$$

where F_g is the free energy of a large enough region in the simulation cell including the GB; N_g is the number of atoms included in that region; F_L is the free energy per atom in the perfect lattice; A is the GB area.

The advantage of QHA is that it is capable to compute the free energy of different phases at temperature ranges where the phases are unstable. Therefore, it can well illustrate the relative stability of different GB phases at different elevated temperatures.

5.1.2 GB Free Energy Computation by Frenkel-Ladd-Path – Complexity of Temperature Induced Behaviors of the Meta-Stable GBs

Frenkel-Ladd-Path (FLP) is a nonequilibrium method to compute the free energy of a system at elevated temperature in a MD simulation. Unlike QHA, it is a process of dynamic simulation to perform thermodynamic integration through a simulated time range. This method has been applied in some systems and proved to have higher accuracy than QHA[83]. However, as the

system is annealed, this method is not capable to compute the free energy of an unstable phase because it will perform phase transition and therefore the computed free energy is no longer of the original phase but of the transformed phase. Therefore, I utilized this method as one of the characters to determine whether GB phases perform phase transition at elevated temperature.

Assume a system with all its atoms doing harmonic vibration near their equilibrium positions $\boldsymbol{r}_i^0$. Its Hamiltonian:

$$H_E = \sum_{i=1}^{N} \frac{\boldsymbol{p}_i^2}{2m} + \sum_{i=1}^{N} \frac{1}{2} m\omega^2 (\boldsymbol{r}_i - \boldsymbol{r}_i^0)^2 \qquad 5\text{-}5$$

This system is also called an Einstein crystal. Using 5-1 and 5-5, construct a new Hamiltonian:

$$H(\lambda) = (1-\lambda)H_0 + \lambda H_E \qquad 5\text{-}6$$

λ is a parameter between 0 and 1. $H(\lambda = 0) = H_0$ and $H(\lambda = 1) = H_E$. Therefore, switching λ between 0 and 1 manipulates the system to be more like its original state or be like an Einstein crystal. The free energy of this $\lambda -$ system is:

$$F(N,V,T;\ \lambda) = -k_B T ln[\frac{1}{h^{3N}} \int d\boldsymbol{r}^N d\boldsymbol{p}^N e^{-\frac{H(\lambda)}{k_B T}}] \qquad 5\text{-}7$$

The derivative of $F(N,V,T;\ \lambda)$ to λ is the canonical ensemble average of $\frac{\partial H(\lambda)}{\partial \lambda}$

$$\frac{\partial F}{\partial \lambda} = \langle \frac{\partial H(\lambda)}{\partial \lambda} \rangle_\lambda \qquad 5\text{-}8$$

Therefore, the free energy difference between λ_i and λ_f – characterized systems is

$$\Delta F = F(\lambda_f) - F(\lambda_i) = \int_{\lambda_i}^{\lambda_f} \langle \frac{\partial H(\lambda)}{\partial \lambda} \rangle_\lambda \, d\lambda \qquad 5\text{-}9$$

In an equilibrium thermodynamic integration method, the system is equilibrated at a series of discrete values of λ, which is costing. Applying the nonequilibrium method proposed by Rodrigo [83] saves much expense. This method relates ΔF to irreversible work which can be effectively computed in a dynamic simulation.

$$\Delta F = W_{iir} - Q \qquad 5\text{-}10$$

where W_{iir} and Q are the irreversible work done to the system and heat dissipated from a specific realization transforming from λ_f to λ_i. When λ_f and λ_i is very close satisfying a

linear-response nonequilibrium process, $Q_{i\to f} \approx Q_{f\to i}$. According to the relationship in Figure 5.1.2 (a), we have

$$\Delta F = F(\lambda_f) - F(\lambda_i) \approx \frac{1}{2}(W_{i\to f} - W_{f\to i}) \qquad 5\text{-}11$$

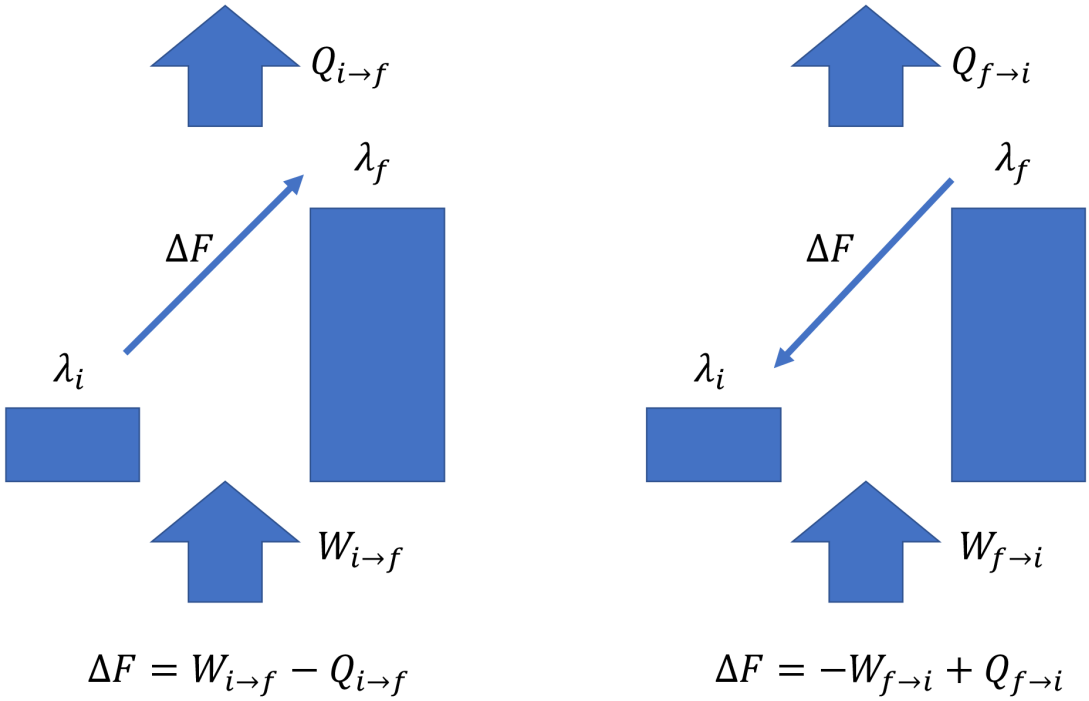

Figure 5.1.2 (a) Relationship between free energy difference, irreversible work and dissipated heat.

The irreversible work $W_{i\to f}$ can be computed along a single simulation where $\lambda(t)$ explicitly varies with time t:

$$W_{i\to f} = \int_0^{t_s} dt \frac{d\lambda}{dt}\left(\frac{\partial H}{d\lambda}\right)_{\boldsymbol{r}^N,\boldsymbol{p}^N} \qquad 5\text{-}12$$

where $\boldsymbol{r}^N, \boldsymbol{p}^N$ represents the phase-space trajectory of the system experiencing this process. Using 5-6, rewrite 5-12 as

$$W_{i\to f} = \int_0^{t_s} dt \frac{d\lambda}{dt}[(H_E)_{\boldsymbol{r}^N,\boldsymbol{p}^N} - (H_0)_{\boldsymbol{r}^N,\boldsymbol{p}^N}] \qquad 5\text{-}13$$

In a real simulation 5-12 is computed numerically:

$$W_{i\to f} = \sum_{n=0}^{N-1} \Delta\lambda_n [(H_E)_{\boldsymbol{r}^N,\boldsymbol{p}^N} - (H_0)_{\boldsymbol{r}^N,\boldsymbol{p}^N}] \qquad 5\text{-}14$$

The process computing $W_{i\to f}$ under molecular simulation is described as below:

1) Manipulate the formula of potential energy as

$$U(\lambda) = (1-\lambda)U_0 + \lambda U_E; \qquad 5\text{-}15$$

with λ varying from 0 to 1 in a time range of t_s which is divided into time step of dt;

2) At each time step, compute $\Delta\lambda_n = \lambda(t) - \lambda(t-dt)$; as the forms of kinetic energy in H_E and H_0 are the same:

$$(H_E)_{\boldsymbol{r}^N,\boldsymbol{p}^N} - (H_0)_{\boldsymbol{r}^N,\boldsymbol{p}^N} = (U_E)_{\boldsymbol{r}^N,\boldsymbol{p}^N} - (U_0)_{\boldsymbol{r}^N,\boldsymbol{p}^N} \qquad 5\text{-}16$$

where $(U_E)_{\boldsymbol{r}^N,\boldsymbol{p}^N}$ and $(U_0)_{\boldsymbol{r}^N,\boldsymbol{p}^N}$ is the potential energy computed by regarding the atoms in the system as interacted by its original atomic potential and as an Einstein crystal respectively with the current atomic positions.

3) Integrate using 5-12.

Figure 5.1.2 (b) illustrates the full process using MD simulation to collect data used to compute $W_{i\to f}$ and $W_{f\to i}$ following the steps above by a single simulation. The initial system at 0K were annealed and maintained to a target temperature T. Then the forward path to compute $W_{H_0\to H_E}$ is executed by varying λ from 0 to 1 in 40000 fs reaching an Einstein crystal state, which is subsequently held by 1000fs. Finally, the backward path to compute $W_{H_E\to H_0}$ is done varying λ from 1 to 0 returning to the H_0 state. Using the data generated by the two paths, the free energy of the system H_0 can be computed following the routine above.

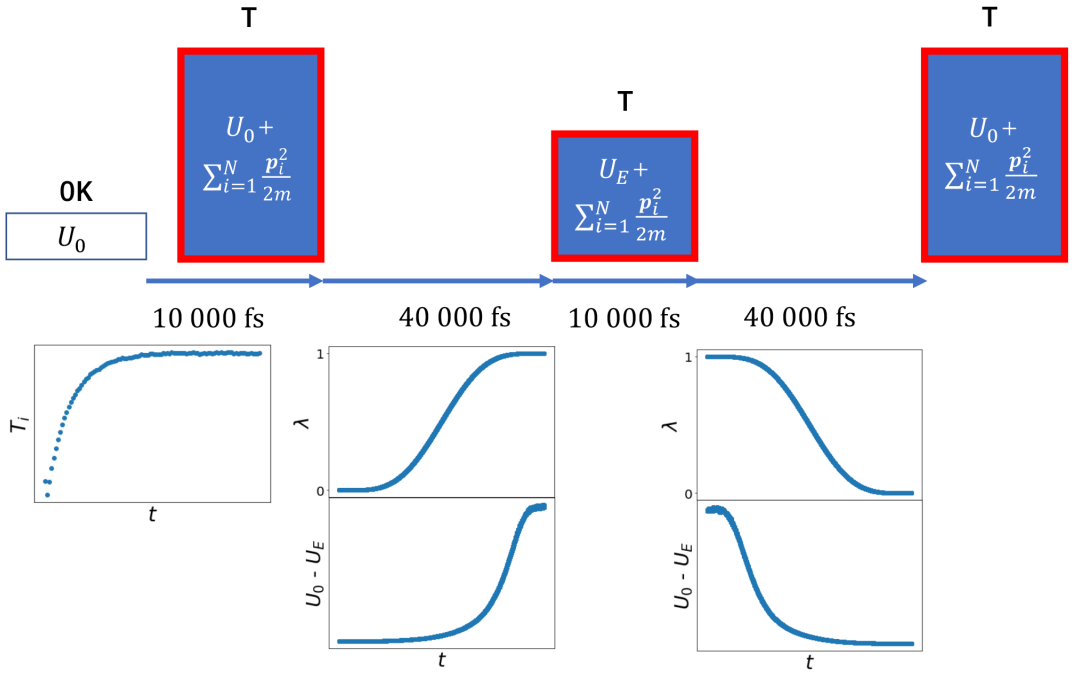

Figure 5.1.2 (b) FLP process in a single MD simulation.

5.1.3 GB Structure Variation Monitored by Steinhart Order Parameters

When being annealed at elevated temperatures, the GB structure with vibrating atoms can be characterized by excess Steinhart Order Parameters[84] (SOPs). The SOPs were proposed by Steinhart which is capable to describe the structural information of an atom with its neighboring atoms. SOPs appear as a set of parameters Q_l and each of them can present a specific atomic environment, which has the form as:

$$\overline{Y}_{lm} = \frac{1}{N}\sum_{j=1}^{N} Y_{lm}(\theta(\mathbf{r}_{ij}), \phi(\mathbf{r}_{ij}))$$
$$Q_l = \sqrt{\frac{4\pi}{2l+1}\sum_{m=-l}^{m=l} \overline{Y}_{lm}\overline{Y}^{*}_{lm}} \qquad 5\text{-}17$$

Q_l is the summation of the contribution of the N atoms surrounding a central atom to their position projections on the spherical harmonics Y_{lm}. Therefore, a specific Q_l parameter characterized by the number l can be applied to analyze the similarity of the distribution of the surrounding atoms to be like a specific type of coordination. For example, a central atom

with a tetragonal coordination environment often has a high Q_3 value. As can be seen in Figure 5.1.3, the averaged Q_l can be applied to monitoring the melting process of a silicon bulk. Q_3 has an abrupt decrease at the melting point, which illustrates an 'abrupt disorder' of the tetragonal coordinated silicon crystal by melting. Also, Q_6 and Q_7 also have an apparent drop at melting point and they can also be applied to characterize certain structural information of silicon lattice. To compute the excess SOPs, the GBs were annealed and maintained at each target temperature for 10000 fs and held by a following 10000 fs to compute the average and standard deviation of the excess SOPs.

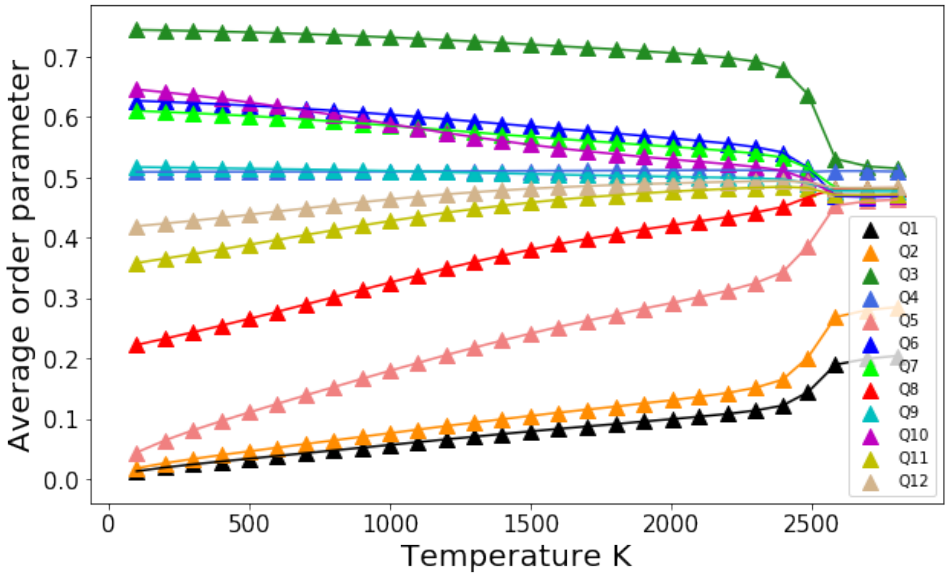

Figure 5.1.3 Variation of the averaged SOPs annealing a silicon bulk to melt

5.2 Results and Discussion

5.2.1 Simulated Thermal Expansion of Silicon Lattice and the Lattice Free Energy by QHA

Figure 5.2.1 (a) shows the thermal expansion of supercell of 18×18×18 replicas of the silicon unit cell including 46656 atoms, which is expressed as a linear CTE respect to the lattice parameter at 300K. As discussed by Purja and Mishin[70], the simulated CTE result is close to the experiment done by Okada & Tokumaru[85]. Though the negative slope over about 1250K is

unphysical, Purja and Mishin have suggested that this will not be a serious limitation because the thermodynamic properties often only depend on the absolute value of the lattice parameter instead of the slope. Indeed, compared with other empirical potentials of silicon, this optimized tersoff potential reflects closer lattice parameters with the experimental results. Figure 5.2.1(b) illustrated the silicon lattice free energy per-atom computed by QHA and HA. Obviously, the effects of thermal expansion on the free energy is not significant. For mediate temperatures, the Tersoff potential well simulate the thermal expansion close to the experiment results. At high temperature, the effects of lattice parameter change on free energy is negligible. Therefore, the computed QHA free energy can be considered as reasonable.

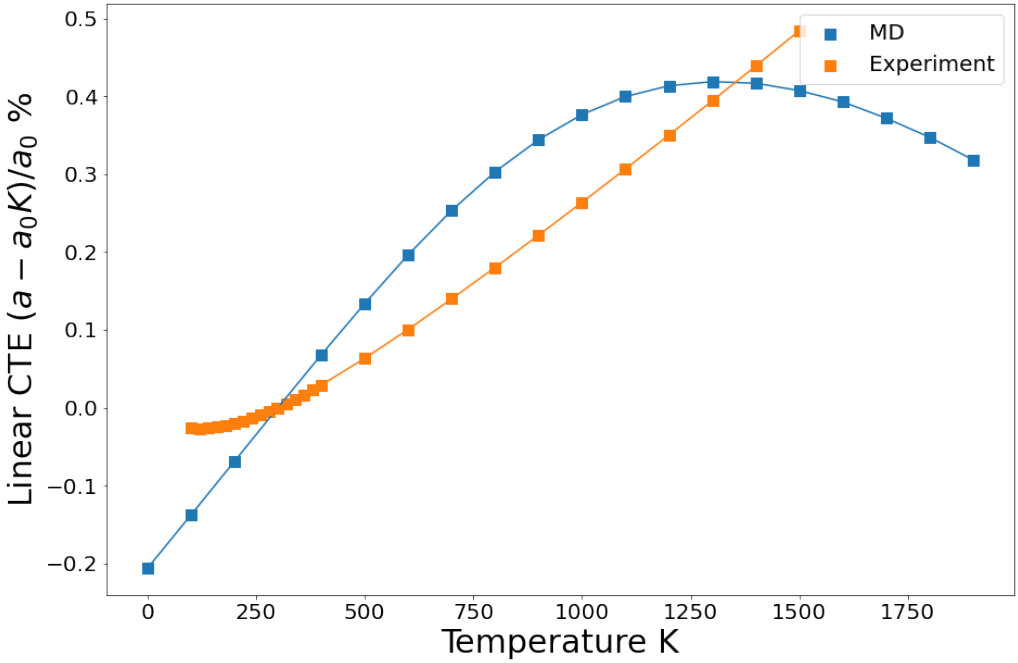

Figure 5.2.1(a) Simulated linear CTE of silicon lattice compared with experiment

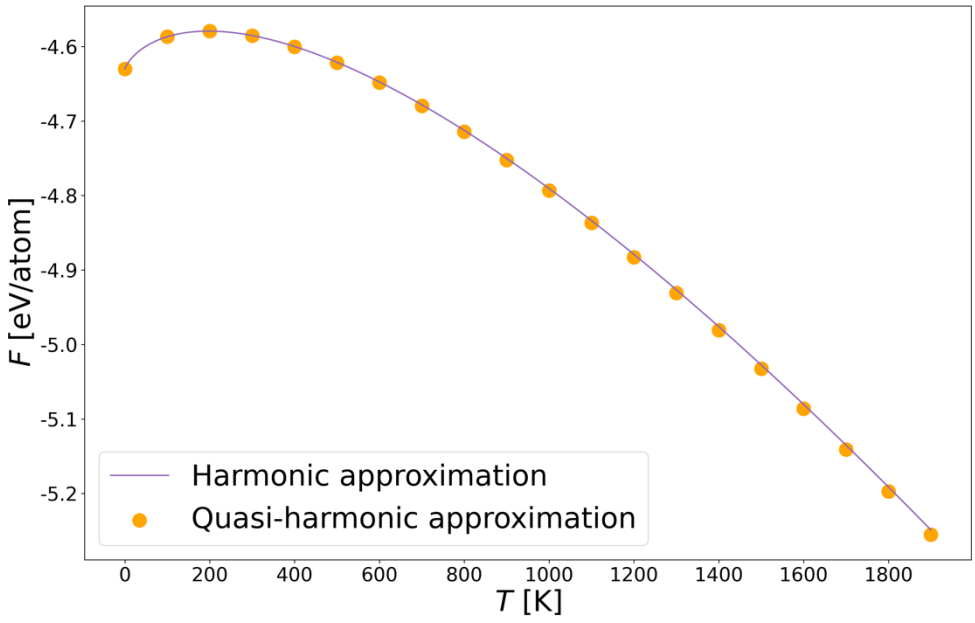

Figure 5.2.1(b) Silicon lattice free energy by QHA and HA

5.2.2 Thermodynamic Stability of GB Phases at Elevated Temperature

This part will be published in journal.

5.2.3 Temperature-Induced Structural Variation of GB Phase and Pre-melting

This part will be published in journal.

5.3 Summary

This part will be published in journal.

6. Phase Transition Mechanism From the Meta-2 to Ground GB Though Localized Structural Reconstruction

As presented in Chapter 5, the Meta-2 GB is capable to transform to a structure being similar like the Ground GB at elevated temperature while the transformed structure was proved to be not identical with the Ground GB. This chapter will explain the reason of this phenomenon by discussing in detail the transformed structure of Meta-2 GB and its transform mechanism.

6.1 Method

6.1.1 Visualizing the Transformed Meta-2 GB

This part will be published in journal.

6.1.2 Computing Transition Barrier by Nudged-Elastic-Band (NEB)

This part will be published in journal.

6.2 Results and Discussion

6.2.1 Phase Transition Mechanism by Localized Structural Reconstruction

This part will be published in journal.

6.2.2 Effects of Neighboring Structural Units on The Kinetic Barrier of Reconstruction

This part will be published in journal.

6.2.3 Effects of disorientation on the GB free energy and entropy

This part will be published in journal.

6.2.4 Dynamic Simulation of the Phase Transition

This part will be published in journal.

6.3 Summary

This part will be published in journal.

7. Electronic Structures of GB Phases

This part will be published in journal.

7.1 Method

This part will be published in journal.

7.2 Result and Discussion

This part will be published in journal.

7.3 Summary

This part will be published in journal.

8. Conclusion

Most materials with important applications in modern times exist as crystalline materials. It still seems to be a long way to eliminate all the barriers to ultimately understand the mechanism of all the crystalline materials' properties due to lacking in a full understand of the effects of crystalline interfaces, which often cause more extensive disparity in properties from the perfect crystal than other defects like point defects or dislocations. Atomic simulation is an effective way to investigate structure-property relationship of interfaces, which is generally needed for both heterogeneous interfaces in modern devices and GBs in many engineering and other cutting-edge applications.

In chapter 2, I introduced a python code which is capable to eliminate two barriers existing in simulation interfaces. One is lacking in an effective and convenient package capable to build a CSL interface by only input crystallographic indices and cif files. Another is lacking in a package capable to compute the cell of non-identical displacement (CNID) of any CSL interface. For the simulation of an interface, it is often required to manipulate the rigid body translation of one crystal respect to the other to sample as wide as possible the GB phase space to avoid only discussing in a narrow region of meta-states. CNID is important because it is the minimum cell including all the rigid body translation (RBT) confined in the interface plane of one crystal respect to the other giving non-identical patterns. The results in this chapter have shown that this package can be conveniently applied to generate both heterogeneous interfaces and grain boundaries of non-cubic lattice system; and the computed CNID can apparently lower the cost of some previous simulations on interfaces and GBs.

An interesting discovery of GB phases is that according to the results from atomic simulation, multiple GB phases seem to commonly exist in GBs of fcc metals. One is capable to explore the GB phases by varying the atomic density near the GB respect to the atomic number in a whole GB plane (GB energy – PAD relationship). The cusps in the GB energy – PAD figure correspond to GB phases which are capable to transform between each other. Similar studies

were subsequently reported in bcc GBs as well. Such a phenomenon was also verified by experimental observation in atomic-scale in an aluminium GB. Despites the exciting achievements in fcc and bcc metals mainly with metallic bonds, it is of both scientific and practical importance to extend this research into other elemental materials. Diamond-structured materials are good candidates to do so. On one hand, their covalent bond character can make new insights of this phenomenon different from the metal GBs. On the other hand, the diamond-structured materials are widely applied in many important modern devices.

Although compared with fcc and bcc GBs, few reported studies have applied the term 'GB phases' on diamond-structured GBs, some properties related to phase behaviors have been discussed. Most atomic simulation explore GB structures at 0 K where a bunch of GB states are often explored. The GB with the lowest GB energy is the most-stable GB while others are meta-stable GBs. Firstly, experiment and simulation results have suggested that silicon GBs can exist as meta-stable states. Secondly, different temperature-induced structural variations have been revealed through atomic simulation in silicon GBs. While compared with fcc and bcc GBs, the atomic simulation often explored far more meta-stable GBs of the diamond-structured GBs, few previous studies have discussed the physical importance of these meta-stable GBs. While it was well accepted that the meta-stable GBs can always transform to the most-stable GB, the temperature-induced behaviors of these meta-stable GBs are still not well investigated. In this situation, some questions remain to be answered. Are these meta-stable GBs explored by an empirical atomic interaction reasonable to exist? Can they become stable at elevated temperature? If not, can they always transform to the most-stable GB? What is the effects of the transition on the physical properties?

Conclusion of the chapters 3-7 will be published in journal.

This research is helpful for more effective interface simulation and has made new insights on understanding the effects of meta-stable GB phases on the properties of materials with covalent bonds.

Appendix

Transformation of Miller indices of the same lattice plane expressed by different bases

It is sometimes convenient to describe lattice planes in a conventional non-primitive lattice while for computation we desire it expressed in a primitive basis. For example, for lattice planes specified by indices (s_{c1}, s_{c2}, s_{c3}) in a conventional lattice $\mathbf{S_c} = [\mathbf{q_{c1}}, \mathbf{q_{c2}}, \mathbf{q_{c3}}]$, we need to derive its indices (s_{p1}, s_{p2}, s_{p3}) expressed in primitive lattice $\mathbf{S_p} = [\mathbf{q_{p1}}, \mathbf{q_{p2}}, \mathbf{q_{p3}}]$.

1) Find three lattice points $\mathbf{P_{c1}}$, $\mathbf{P_{c2}}$, $\mathbf{P_{c3}}$ belonging to one of the (s_{c1}, s_{c2}, s_{c3}) lattice planes. Firstly, select one index $s_{ci} \neq 0$ with its corresponding vector $\mathbf{q}_{ci}$ and one of the three points $\mathbf{P}_{c1}$ as:

$$\mathbf{P}_{c1} = \frac{\mathbf{q}_{ci}}{s_{ci}} \ (s_{ci} \neq 0) \ (i = 1,2,3)$$

Then

$$\mathbf{P}_{c2}, \mathbf{P}_{c3} = \begin{cases} \mathbf{P}_{c1} + \mathbf{q}_{cj} & (s_{cj} = 0) \\ \dfrac{\mathbf{q}_{cj}}{s_{cj}} & (s_{cj} \neq 0) \end{cases} \quad (j = 1,2,3 \ \& \ j \neq i)$$

The normal to the plane $\mathbf{n}$ is:

$$\mathbf{n} = (\mathbf{P}_{c1} - \mathbf{P}_{c2}) \times (\mathbf{P}_{c1} - \mathbf{P}_{c3})$$

For any points $\mathbf{P}_x$ located in this plane we have:

$$(\mathbf{P}_x - \mathbf{P}_{c1}) \cdot \mathbf{n} = 0$$

2) Determined s_{pi} by substitute $\mathbf{P}_x$ by $\mathbf{q}_{pi}/s_{pi}$ into $(\mathbf{P}_x - \mathbf{P}_{c1}) \cdot \mathbf{n} = 0$

$$s_{pi} = \frac{\mathbf{q}_{pi} \cdot \mathbf{n}}{\mathbf{P}_{c1} \cdot \mathbf{n}}$$

Note that this method can be used to convert the Miller indices of certain lattice plane expressed in any two overlapping lattices.

Acknowledgements

I would like to express my great appreciation to my supervisor Professor Teruyasu Mizoguchi. He has provided me with not only extensive help in research resources but also with greatly important advices in my research. Professor Mizoguchi is a so kind person that I have really enjoyed the atmosphere in the lab. I also need to thank Dr Kiyou Shibata who has helped me a lot in technical aspects. I also really appreciate their extensive work on reviewing my presentation and academical writing. I could not have gone this far without their help. Additionally, I appreciate the Japanese and Chinese government for giving me opportunity to be totally supported for my PhD programme by Ministry of Education, Culture, Sports, Science and Technology (MEXT) with Embassy Recommendation for Chinese students. Finally, I really appreciate the financial and spiritual support from my parents in the past three years. This work was supported by the MEXT; Nos 17H06094,19H00818, 19H05787, and 18K14117 and CREST (JPMJCR1993). I acknowledge to Prof. Atsuo Seko at Kyoto University, Prof. Susumu Fujii at Osaka University, and Dr. Masanori Kohyama at AIST for their helpful discussions on the silicon simulations.

Reference

1. SUTTON & P., A. Interfaces in Crystalline Materials. *Monogr. Physice Chem. Mater.* 414–423 (1995).
2. Kroemer, H. Nobel Lecture: Quasielectric fields and band offsets: teaching electrons new tricks. *Rev. Mod. Phys.* **73**, 783 (2001).
3. Pervez, S. A., Cambaz, M. A., Thangadurai, V. & Fichtner, M. Interface in Solid-State Lithium Battery: Challenges, Progress, and Outlook. *ACS Appl. Mater. Interfaces* **11**, 22029–22050 (2019).
4. Chen, H., Zhang, W., Li, M., He, G. & Guo, X. Interface Engineering in Organic Field-Effect Transistors: Principles, Applications, and Perspectives. *Chem. Rev.* **120**, 2879–2949 (2020).
5. Gariglio, S., Gabay, M., Mannhart, J. & Triscone, J. M. Interface superconductivity. *Phys. C Supercond. its Appl.* **514**, 189–198 (2015).
6. Watanabe, T. Grain boundary engineering: Historical perspective and future prospects. in *Journal of Materials Science* vol. 46 4095–4115 (Springer, 2011).
7. Broqvist, P., Alkauskas, A., Godet, J. & Pasquarello, A. First principles investigation of defect energy levels at semiconductor-oxide interfaces: Oxygen vacancies and hydrogen interstitials in the Si–SiO2–HfO2 stack. *J. Appl. Phys.* **105**, 061603 (2009).
8. Markov, S. *et al.* Atomic level modeling of extremely thin silicon-on-insulator MOSFETs including the silicon dioxide: Electronic structure. *IEEE Trans. Electron Devices* **62**, 696–704 (2015).
9. Tanner, C. M., Choi, J. & Chang, J. P. Electronic structure and band alignment at the HfO2/4H-SiC interface. *J. Appl. Phys.* **101**, 034108 (2007).
10. Blom, A. & Stokbro, K. Atomistic modeling of semiconductor interfaces. *J. Comput. Electron.* **12**, 623–637 (2013).
11. Tschopp, M. A. & McDowell, D. L. Asymmetric tilt grain boundary structure and energy in copper and aluminium. *Philos. Mag.* **87**, 3871–3892 (2007).

12. Olmsted, D. L., Foiles, S. M. & Holm, E. A. Survey of computed grain boundary properties in face-centered cubic metals: I. Grain boundary energy. *Acta Mater.* **57**, 3694–3703 (2009).

13. Homer, E. R., Patala, S. & Priedeman, J. L. Grain Boundary Plane Orientation Fundamental Zones and Structure-Property Relationships. *Sci. Rep.* **5**, 1–13 (2015).

14. Oda, H., Kiyohara, S. & Mizoguchi, T. Machine learning for structure determination and investigating the structure-property relationships of interfaces. *JPhys Mater.* **2**, 34005 (2019).

15. Huber, L., Hadian, R., Grabowski, B. & Neugebauer, J. ARTICLE OPEN A machine learning approach to model solute grain boundary segregation. *npj Comput. Mater.* **4**, 64 (2018).

16. Olmsted, D. L., Holm, E. A. & Foiles, S. M. Survey of computed grain boundary properties in face-centered cubic metals—II: Grain boundary mobility. *Acta Mater.* **57**, 3704–3713 (2009).

17. Frolov, T., Olmsted, D. L., Asta, M. & Mishin, Y. Structural phase transformations in metallic grain boundaries. *Nat. Commun.* **4**, 1899 (2013).

18. Frolov, T. *et al.* Grain boundary phases in bcc metals. *Nanoscale* **10**, 8253–8268 (2018).

19. Zhu, Q., Samanta, A., Li, B., Rudd, R. E. & Frolov, T. Predicting phase behavior of grain boundaries with evolutionary search and machine learning. *Nat. Commun.* **9**, 1–9 (2018).

20. Hadian, R., Grabowski, B., Finnis, M. W. & Neugebauer, J. Migration mechanisms of a faceted grain boundary. *Phys. Rev. Mater.* **2**, 43601 (2018).

21. Banadaki, A. D. & Patala, S. A simple faceting model for the interfacial and cleavage energies of Σ3 grain boundaries in the complete boundary plane orientation space. *Comput. Mater. Sci.* **112**, 147–160 (2016).

22. Abdeljawad, F. & Foiles, S. M. Stabilization of nanocrystalline alloys via grain boundary segregation: A diffuse interface model. *Acta Mater.* **101**, 159–171 (2015).

23. Priedeman, J. L. & Thompson, G. B. The influence of alloying in stabilizing a faceted grain boundary structure. *Acta Mater.* **201**, 329–340 (2020).

24. Brandon, D. G. The structure of high-angle grain boundaries. *Acta Metall.* **14**, 1479–1484 (1966).

25. Ranganathan, S. On the geometry of coincidence-site lattices. *Acta Crystallogr.* **21**, 197–199 (1966).

26. Bollmann, W. General Geometrical Theory of Crystalline Interfaces. in *Crystal Defects and Crystalline Interfaces* 143–185 (Springer Berlin Heidelberg, 1970). doi:10.1007/978-3-642-49173-3_12.

27. Author, B., Pond, R. C. & Vlachavas, D. S. *Bicrystallography*. *Source: Proceedings of the Royal Society of London. Series A, Mathematical and Physical Sciences* vol. 386 https://about.jstor.org/terms (1983).

28. Bristowe, P. D., Brokman, A., Spaepen, F. & Balluffi, R. W. Simulation of the structure of vacancies in high angle grain boundaries. (1980) doi:10.2172/5054255.

29. Chen, S. P., Voter, A. F. & Srolovitz, D. J. Computer simulation of grain boundaries in Ni/sub 3/Al: The effect of grain boundary composition. *Scr. Metall.* **20**, 1389–1394 (1986).

30. Kluge, M. D., Wolf, D., Lutsko, J. F. & Phillpot, S. R. Formalism for the calculation of local elastic constants at grain boundaries by means of atomistic simulation. *J. Appl. Phys.* **67**, 2370 (1998).

31. Duffy, D. M. Grain boundaries in ionic crystals. *J. Phys. C Solid State Phys.* **19**, 4393 (1986).

32. Duffy, D. M. & Tasker, P. W. Computer simulation of grain boundaries in ionic crystals. *Phys. B+C* **131**, 46–52 (1985).

33. Majid, I. & Bristowe, P. D. Dynamical simulation of structural multiplicity in grain boundaries. *dssm* (1987).

34. Priester, L. Grain Boundaries: From Theory to Engineering. *Grain Boundaries* **172**, 217–240 (2013).

35. Raghunathan, R., Johlin, E. & Grossman, J. C. Grain boundary engineering for improved thin silicon photovoltaics. *Nano Lett.* **14**, 4943–4950 (2014).

36. Schneider, M., Rahman, A. & Schuller, I. K. Epitaxial growth of thin films studied by molecular dynamics simulation. *Superlattices Microstruct.* **7**, 39–46 (1990).

37. Das Sarma, S., Marmorkos, I. K. & Paik, S. M. Numerical simulation studies of epitaxial thin film growth modes and mechanisms. *Surf. Sci.* **228**, 28–32 (1990).

38. Dregia, S. A. & Ahmed, S. Equilibrium Segregation and Dislocation Structures at Epitaxial Interphase Boundaries. *PhDT* (1989).

39. Legoues, F. K., Krakow, W. & Ho, P. S. Atomic structure of the epitaxial Al–Si interface. *http://dx.doi.org/10.1080/01418618608245295* **53**, 833–841 (2006).

40. Hadian, R., Grabowski, B. & Neugebauer, J. GB code: A grain boundary generation code Software • Review • Repository • Archive. (2018) doi:10.21105/joss.00900.

41. Cheng, J., Luo, J. & Yang, K. Aimsgb: An algorithm and open-source python library to generate periodic grain boundary structures. *Comput. Mater. Sci.* **155**, 92–103 (2018).

42. Mathew, K. *et al.* MPInterfaces: A Materials Project based Python tool for high-throughput computational screening of interfacial systems. *Comput. Mater. Sci.* **122**, 183–190 (2016).

43. Ong, S. P. *et al.* Python Materials Genomics (pymatgen): A robust, open-source python library for materials analysis. *Comput. Mater. Sci.* **68**, 314–319 (2013).

44. Hickman, J. & Mishin, Y. Extra variable in grain boundary description. *RAPID Commun. Phys. Rev. Mater.* **1**, 10601 (2017).

45. Banadaki, A. D., Tschopp, M. A. & Patala, S. An efficient Monte Carlo algorithm for determining the minimum energy structures of metallic grain boundaries. *Comput. Mater. Sci.* **155**, 466–475 (2018).

46. Zhu, Q., Samanta, A., Li, B., Rudd, R. E. & Frolov, T. Predicting phase behavior of grain boundaries with evolutionary search and machine learning. *Nat. Commun.* **9**, 1–9 (2018).

47. Kiyohara, S., Oda, H., Tsuda, K. & Mizoguchi, T. Acceleration of stable interface structure searching using a kriging approach. *Jpn. J. Appl. Phys.* **55**, 45502 (2016).

48. Oda, H., Kiyohara, S., Tsuda, K. & Mizoguchi, T. Transfer learning to accelerate interface structure searches. *J. Phys. Soc. Japan* **86**, (2017).

49. Pond, R. C. *Periodic Grain Boundary Structures in Aluminium. II. A Geometrical Method for Analysing Periodic Grain Boundary Structure and some Related Transmission Electron Microscope Observations*. *Source: Proceedings of the Royal Society of London. Series A, Mathematical and Physical Sciences* vol. 357 https://www.jstor.org/stable/79398 (1977).

50. Han, J., Thomas, S. L. & Srolovitz, D. J. Grain-Boundary Kinetics: A Unified Approach. (2018) doi:10.1016/j.pmatsci.2018.05.004.

51. Divinski, S. V., Edelhoff, H. & Prokofjev, S. Diffusion and segregation of silver in copper Σ5(310) grain boundary. *Phys. Rev. B - Condens. Matter Mater. Phys.* **85**, 144104 (2012).

52. Cantwell, P. R. *et al.* Grain Boundary Complexion Transitions. *Annu. Rev. Mater. Res.* **50**, (2020).

53. Krause, A. R. *et al.* Review of grain boundary complexion engineering: Know your boundaries. *J. Am. Ceram. Soc.* **102**, jace.16045 (2018).

54. Meiners, T., Frolov, T., Rudd, R. E., Dehm, G. & Liebscher, C. H. Observations of grain-boundary phase transformations in an elemental metal. *Nature* **579**, 375–378 (2020).

55. Frolov, T. *et al.* Grain boundary phases in bcc metals. *Nanoscale* **10**, 8253–8268 (2018).

56. Frolov, T., Olmsted, D. L., Asta, M. & Mishin, Y. Structural phase transformations in metallic grain boundaries. *Nat. Commun.* **4**, 1–7 (2013).

57. Hickman, J. & Mishin, Y. Extra variable in grain boundary description. *Phys. Rev. Mater.* **1**, 010601 (2017).

58. Raghunathan, R., Johlin, E. & Grossman, J. C. Grain boundary engineering for improved thin silicon photovoltaics. *Nano Lett.* **14**, 4943–4950 (2014).

59. Mohr, M. *et al.* Influence of grain boundaries on elasticity and thermal conductivity of nanocrystalline diamond films. *Acta Mater.* **122**, 92–98 (2017).

60. Takeuchi, W. *et al.* High hole mobility tin-doped polycrystalline germanium layers formed on insulating substrates by low-temperature solid-phase crystallization. *Appl. Phys. Lett.* **107**, 22103 (2015).

61. Han, J., Vitek, V. & Srolovitz, D. J. Grain-boundary metastability and its statistical properties. *Acta Mater.* **104**, 259–273 (2016).

62. Kohyama, M., Yamamoto, R. & Doyama, M. Reconstructed Structures of Symmetrical 〈011〉 Tilt Grain Boundaries in Silicon. *Phys. status solidi* **138**, 387–397 (1986).

63. Von Alfthan, S., Haynes, P. D., Kaski, K. & Sutton, A. P. Are the Structures of Twist Grain Boundaries in Silicon Ordered at 0 K? (2006) doi:10.1103/PhysRevLett.96.055505.

64. von Alfthan, S., Kaski, K. & Sutton, A. P. Molecular dynamics simulations of temperature-induced structural transitions at twist boundaries in silicon. *Phys. Rev. B* **76**, 245317 (2007).

65. Wang, L., Yu, W. & Shen, S. Revisiting the structures and energies of silicon â©110) symmetric tilt grain boundaries. *J. Mater. Res.* **34**, 1021–1033 (2019).

66. Sakaguchi, N., Ichinose, H. & Watanabe, S. Atomic Structure of Faceted Σ3 CSL Grain Boundary in Silicon: HRTEM and <I>Ab-initio</I> Calculation. *Mater. Trans.* **48**, 2585–2589 (2007).

67. Plimpton, S. Fast parallel algorithms for short-range molecular dynamics. *J. Comput. Phys.* **117**, 1–19 (1995).

68. Mishin, Y., Farkas, D., Mehl, M. J. & Papaconstantopoulos, D. A. Interatomic potentials for monoatomic metals from experimental data and ab initio calculations. *Phys. Rev. B - Condens. Matter Mater. Phys.* **59**, 3393–3407 (1999).

69. Erhart, P. & Albe, K. Analytical potential for atomistic simulations of silicon, carbon, and silicon carbide. *Phys. Rev. B - Condens. Matter Mater. Phys.* **71**, 035211 (2005).

70. Pun, G. P. P. & Mishin, Y. Optimized interatomic potential for silicon and its application to thermal stability of silicene. *Phys. Rev. B* **95**, 224103 (2017).

71. Tersoff, J. Modeling solid-state chemistry: Interatomic potentials for multicomponent systems. *Phys. Rev. B* **39**, 5566–5568 (1989).

72. Los, H. & Fasolino, A. Intrinsic long-range bond-order potential for carbon: Performance in Monte Carlo simulations of graphitization. *Phys. Rev. B - Condens. Matter Mater. Phys.* **68**, 024107 (2003).

73. Ratanaphan, S., Yoon, Y. & Rohrer, G. S. The five parameter grain boundary character distribution of polycrystalline silicon. *J. Mater. Sci. 2014 4914* **49**, 4938–4945 (2014).

74. Zhu, Q., Samanta, A., Li, B., Rudd, R. E. & Frolov, T. Predicting phase behavior of grain boundaries with evolutionary search and machine learning. doi:10.1038/s41467-018-02937-2.

75. Frolov, T. & Mishin, Y. Thermodynamics of coherent interfaces under mechanical stresses. II. Application to atomistic simulation of grain boundaries. *Phys. Rev. B - Condens. Matter Mater. Phys.* **85**, 224107 (2012).

76. Han, J., Vitek, V. & Srolovitz, D. J. Grain-boundary metastability and its statistical properties. *Acta Mater.* **104**, 259–273 (2016).

77. Kohyama, M. & Yamamoto, R. Theoretical study of grain boundaries in Si: Effects of structural disorder on the local electronic structure and the origin of band tails. *Phys. Rev. B* **50**, 8502–8522 (1994).

78. Kohyama, M., Yamamoto, R. & Doyama, M. Structures and Energies of Symmetrical 〈011〉 Tilt Grain Boundaries in Silicon. *Phys. status solidi* **137**, 11–20 (1986).

79. Kresse, G. & Furthmüller, J. Efficient iterative schemes for *ab initio* total-energy calculations using a plane-wave basis set. *Phys. Rev. B* **54**, 11169 (1996).

80. Kresse, G. & Joubert, D. From ultrasoft pseudopotentials to the projector augmented-wave method. *Phys. Rev. B* **59**, 1758 (1999).

81. Frolov, T. *et al.* Grain boundary phases in bcc metals. *Nanoscale* **10**, 8253–8268 (2018).

82. Freitas, R., Rudd, R. E., Asta, M. & Frolov, T. Free energy of grain boundary phases: Atomistic calculations for Σ5(310)[001] grain boundary in Cu. *Phys. Rev. Mater.* **2**, 093603 (2018).

83. Freitas, R., Asta, M. & De Koning, M. Nonequilibrium free-energy calculation of solids using LAMMPS. *Comput. Mater. Sci.* **112**, 333–341 (2016).

84. Steinhardt, P. J., Nelson, D. R. & Ronchetti, M. *Bond-orientational order in liquids and glasses*. *PHYSICAL REVIEW B* vol. 28 (1983).

85. Okada, Y. & Tokumaru, Y. Precise determination of lattice parameter and thermal expansion coefficient of silicon between 300 and 1500 K. *JAP* **56**, 314–320 (1984).

86. Stukowski, A. Visualization and analysis of atomistic simulation data with OVITO-the Open Visualization Tool. *Model. Simul. Mater. Sci. Eng.* **18**, (2010).

87. Henkelman, G. & Jónsson, H. Improved tangent estimate in the nudged elastic band method for finding minimum energy paths and saddle points. *J. Chem. Phys.* **113**, 9978 (2000).

88. Henkelman, G., Uberuaga, B. P. & Jónsson, H. A climbing image nudged elastic band method for finding saddle points and minimum energy paths. *J. Chem. Phys.* **113**, 9901 (2000).

89. Maras, E., Trushin, O., Stukowski, A., Ala-Nissilä, T. & Jónsson, H. Global transition path search for dislocation formation in Ge on Si(001). *Comput. Phys. Commun.* **205**, 13–21 (2016).

90. Momma, K. & Izumi, F. VESTA: a three-dimensional visualization system for electronic and structural analysis. *urn:issn:0021-8898* **41**, 653–658 (2008).

91. Kohyama, M. & Yamamoto, R. *Theoretical study of grain boundaries in Si: EÃects of structural disorder on the local electronic structure and the origin of band tails*. *PHYSICAL REVIEW B* vol. 50.

List of Publications

Journal Papers

1. Xie Y, Shibata K, Miozguchi T. A brute-force code searching for cell of non-identical displacement for CSL grain boundaries and interfaces[J]. Computer Physics Communications, 2021: 108260.

2. Integrated structural reconstruction of unit structures of the meta-stable grain boundaries in diamond-structured materials presents first-order like phase transition. Will submit soon.

3. *Interface_Master* – a python package building CSL or approximate CSL interfaces of any two lattices and effectively computing cell of non-identical displacement (CNID), Will submit soon.

4. Atomic simulation on the photovoltaic properties of GaAs grain boundaries. In preparation

Conference

1. Phase transition of a meta-stable structure of a symmetrical tilt grain boundary in diamond-structured materials - The Ceramic Society of Japan Annual Meeting 2021

2. Grain Boundary Meta-Stable Phases and the Phase Transition by Structural-Reconstruction in Diamond-Structured Materials - 8th International Congress on Ceramics 2021

3. Determination of Stable and Meta-stable Grain Boundary Phases in Diamond-structured Materials – The Japan Institute of Metals and Materials Spring Meeting 2021